BRAININFO 2016

The First International Conference on Neuroscience and Cognitive Brain Information

ISBN: 978-1-61208-526-5

November 13 - 17, 2016

Barcelona, Spain

BRAININFO 2016 Editors

Pengyu Hong, Brandeis University, USA

Birgit Gersbeck-Schierholz, Leibniz Universität Hannover, Germany

BRAININFO 2016

Foreword

The First International Conference on Neuroscience and Cognitive Brain Information (BRAININFO 2016), held between November 13-17, 2016 - Barcelona, Spain was dedicated to evaluate current achievements and identify potential ways of making use of the acquired knowledge, covering, the neuroscience, brain connectivity, brain intelligence paradigms, cognitive information, and specific applications.

Complexity of the human brain and its cognitive actions stimulated many researches for decades. Most of the findings were adapted in virtual/artificial systems in the idea of brain-like modeling them and used in human-centered medical cures, especially for neurotechnologies. Information representation, retrieval, and internal data connections still constitutes a domain where solutions are either missing or in a very early stage.

We take here the opportunity to warmly thank all the members of the BRAININFO 2016 Technical Program Committee, as well as the numerous reviewers. The creation of such a high quality conference program would not have been possible without their involvement. We also kindly thank all the authors who dedicated much of their time and efforts to contribute to BRAININFO 2016. We truly believe that, thanks to all these efforts, the final conference program consisted of top quality contributions.

Also, this event could not have been a reality without the support of many individuals, organizations, and sponsors. We are grateful to the members of the BRAININFO 2016 organizing committee for their help in handling the logistics and for their work to make this professional meeting a success.

We hope that BRAININFO 2016 was a successful international forum for the exchange of ideas and results between academia and industry and for the promotion of progress in the area of neuroscience and cognitive brain information.

We are convinced that the participants found the event useful and communications very open. We also hope the attendees enjoyed the charm of Barcelona, Spain.

BRAININFO 2016 Chairs:

BRAININFO 2016 Advisory Committee

Marius George Linguraru, Children's National Medical Center | George Washington University School of Medicine and Health Sciences, Washington D.C., USA
Pengyu Hong, Brandeis University, USA
Erwin Lemche, Institute of Psychiatry, Psychology & Neuroscience | King's College School of Medicine and Dentistry, UK
Ramesh Krishnamurthy, Health Systems and Innovation Cluster, World Health Organization - Geneva, Switzerland
Irini Giannopulu, Pierre & Marie Curie University - Paris VI, France

BRAININFO 2016

Committee

BRAININFO 2016 Advisory Committee

Marius George Linguraru, Children's National Medical Center | George Washington University School of Medicine and Health Sciences, Washington D.C., USA
Pengyu Hong, Brandeis University, USA
Erwin Lemche, Institute of Psychiatry, Psychology & Neuroscience | King's College School of Medicine and Dentistry, UK
Ramesh Krishnamurthy, Health Systems and Innovation Cluster, World Health Organization - Geneva, Switzerland
Irini Giannopulu, Pierre & Marie Curie University - Paris VI, France

BRAININFO 2016 Technical Program Committee

Hervé Abdi, The University of Texas at Dallas, USA
Murat Akcakaya, University of Pittsburgh, USA
Sergio Cruces, University of Seville, Spain
Deniz Erdogmus, Northeastern University, USA
Irini Giannopulu, Pierre & Marie Curie University - Paris VI, France
Christoph Guger, g.tec medical engineering GmbH, Austria
Pengyu Hong, Brandeis University, USA
Nuri Firat Ince, University of Houston, USA
Nikola Kasabov, Auckland University of Technology, New Zealand
Ramesh Krishnamurthy, Health Systems and Innovation Cluster, World Health Organization - Geneva, Switzerland
Elmar W. Lang, Institute of Biophysics - University of Regensburg, Germany
Erwin Lemche, Institute of Psychiatry, Psychology & Neuroscience | King's College School of Medicine and Dentistry, UK
Marius George Linguraru, Children's National Medical Center | George Washington University School of Medicine and Health Sciences, Washington D.C., USA
Wentai Liu, California NanoSystems Institute (CNSI) | Brain Research Institute (BRI) | University of California at Los Angeles (UCLA), USA
Pinaki Sarder, University at Buffalo - The State University of New York, USA
Andrzej Skowron, Institute of Mathematics - University of Warsaw, Poland
Ricardo Vigário, University Nova of Lisbon, Portugal
Wenwu Wang, University of Surrey, UK
R. Suzanne Zukin, Albert Einstein College of Medicine, USA

Copyright Information

For your reference, this is the text governing the copyright release for material published by IARIA.

The copyright release is a transfer of publication rights, which allows IARIA and its partners to drive the dissemination of the published material. This allows IARIA to give articles increased visibility via distribution, inclusion in libraries, and arrangements for submission to indexes.

I, the undersigned, declare that the article is original, and that I represent the authors of this article in the copyright release matters. If this work has been done as work-for-hire, I have obtained all necessary clearances to execute a copyright release. I hereby irrevocably transfer exclusive copyright for this material to IARIA. I give IARIA permission or reproduce the work in any media format such as, but not limited to, print, digital, or electronic. I give IARIA permission to distribute the materials without restriction to any institutions or individuals. I give IARIA permission to submit the work for inclusion in article repositories as IARIA sees fit.

I, the undersigned, declare that to the best of my knowledge, the article is does not contain libelous or otherwise unlawful contents or invading the right of privacy or infringing on a proprietary right.

Following the copyright release, any circulated version of the article must bear the copyright notice and any header and footer information that IARIA applies to the published article.

IARIA grants royalty-free permission to the authors to disseminate the work, under the above provisions, for any academic, commercial, or industrial use. IARIA grants royalty-free permission to any individuals or institutions to make the article available electronically, online, or in print.

IARIA acknowledges that rights to any algorithm, process, procedure, apparatus, or articles of manufacture remain with the authors and their employers.

I, the undersigned, understand that IARIA will not be liable, in contract, tort (including, without limitation, negligence), pre-contract or other representations (other than fraudulent misrepresentations) or otherwise in connection with the publication of my work.

Exception to the above is made for work-for-hire performed while employed by the government. In that case, copyright to the material remains with the said government. The rightful owners (authors and government entity) grant unlimited and unrestricted permission to IARIA, IARIA's contractors, and IARIA's partners to further distribute the work.

Table of Contents

Classification of Hand Flexion/Extension Using High-density ECoG

Tianxiao Jiang, Tao Jiang, Taylor Wang, Shenshen Mei, Qingzhu Liu, Yunlin Li,
Xiaofei Wang, Sujit Prabhu, Zhiyi Sha, Nuri F. Ince*
*Department of Biomedical Engineering,
University of Houston, Houston, Texas, USA 77204–5060
Email: nfince@uh.edu

***Abstract*—Grasping is one of the most important hand movements performed in daily life and therefore a hand neuroprosthetic should be able to achieve this function with high accuracy. Electrocorticogram (ECoG) recorded from standard clinical electrodes has been proposed as a potential control signal in brain-machine interfaces (BMIs) and used to provide information about executed motor activity such as arm movement direction and individual finger movements. Here, we investigate the value of ECoG recorded from human motor cortex with high density electrodes to distinguish between hand flexion and extension in single trial level for a hand neuroprosthetic. Two subjects were asked to execute spontaneous hand extension and flexion during the recording. Event-related desynchronization (ERD) and event-related synchronization (ERS) in low-frequency band (LFB: 8-32 Hz) and high-frequency band (HFB: 60-200 Hz) were observed in both subjects during these executed movements. ECoG signal was bandpass filtered in three subbands, alpha (8-13 Hz), beta (13-32 Hz) and gamma (60-200 Hz) for classification. A common spatial pattern (CSP) algorithm fused with linear discriminant analysis (LDA) was used to distinguish between executed movements. In both subjects, the gamma band yielded classification accuracies close to 100%. Alpha and beta bands provided poor classification results with higher latency compared to gamma band. These results suggested that the gamma band spatial patterns of motor cortex captured with high-density ECoG can effectively distinguish between hand extension and flexion. High-density ECoG can be a promising modality to drive a neural prosthetic which can help paralyzed patients to regain crucial daily hand functions.**

Keywords*—*High-density ECoG; Time-frequency map; CSP; LDA.

I. INTRODUCTION

ECoG was initially performed in clinical setting to determine the extent of resection in epilepsy cases intraoperatively [1][2]. Nowadays, ECoG is used not only for clinical decision making but also in BMI studies to establish the communication and control function. Compared to scalp electroencephalogram (EEG), the ECoG provides higher signal quality and wider bandwidth as it is recorded directly from the cortex.

Previous studies have found that sensorimotor activity is correlated with the power changes in specific subbands of ECoG [3]. Amplitude modulations in gamma band (40-200 Hz) were found to be closely related to motor behaviors. In the past few years, features extracted from the gamma range of ECoG or local field potentials have been extensively used to decode hand movements of both human and non-human primates [4]–[6]. Previous ECoG based BMI studies generally use large clinical grids with an inter-electrode spacing of 10 mm. With the advancements in micro electrode technology today, the spatial resolution of ECoG has dramatically increased. Recent studies have just started to show the potential of high-density ECoG in decoding human motor functions including cursor control [7], differentiation between multiple hand gestures [5] and to drive a prosthetic limb online [8].

In this study we explored the spatial patterns of ECoG recorded from two subjects during hand flexion and extension tasks. In particular, a customized high-density grid with 120 channels (12×10, 1.2 mm contact exposure and 4 mm spacing) was used to assess cortical activity with superior resolution compared to clinical electrodes with 10mm contact spacing. We characterized the time-frequency dynamics and investigated to what extend the recorded activity can be used to distinguish between hand extension and flexion to drive a neuroprosthetic. In detail, we studied the contribution of ECoG subbands to the classification of the executed tasks. Moreover, rather than focusing on grasping only, we focused on the differentiation between hand flexion and extension to improve the functions of a hand prosthetic and aimed to answer the question whether these activities are associated with different patterns in ECoG.

II. MATERIALS AND METHODS

Below we describe the experimental setup and signal processing techniques used in this study.

A. Experimental setup

A customized 120 (12×10) channel high-density electrode grid with a contact diameter of 1.2 mm and inter-electrode distance of 4 mm was used in this study. The electrodes were placed on the cortex of two subjects who require functional mapping and monitoring during awake brain surgery. The ECoG were intraoperatively recorded along with forearm EMG and bipolar ECG (lead-II) for 15-20 mins period with a 2 kHz sampling frequency and 16 bit A/D resolution. During the recordings, the subjects were asked to perform hand extension/flexion according to auditory instructions. Each movement type was executed for 30 times and followed by 2-3 seconds resting period. Hand movements and the finger positions were digitized by a digital glove. The finger position data provided by the digital glove are further synchronized with the ECoG via simultaneously recorded trigger signal. The details of the system setup were described in [9].

B. Time-frequency maps

ECoG data were manually scrutinized to exclude bad channels. A series of FIR notch filters were applied to suppress 50 Hz power line noise and its harmonics up to 200 Hz. The movement onsets were annotated according to the changes in finger positions and EMG data. The ECoG data were aligned with respect to movement onset and each trial consisted three seconds of data centered at movement onset (1.5s before and

 ISBN: 978-1-61208-526-5

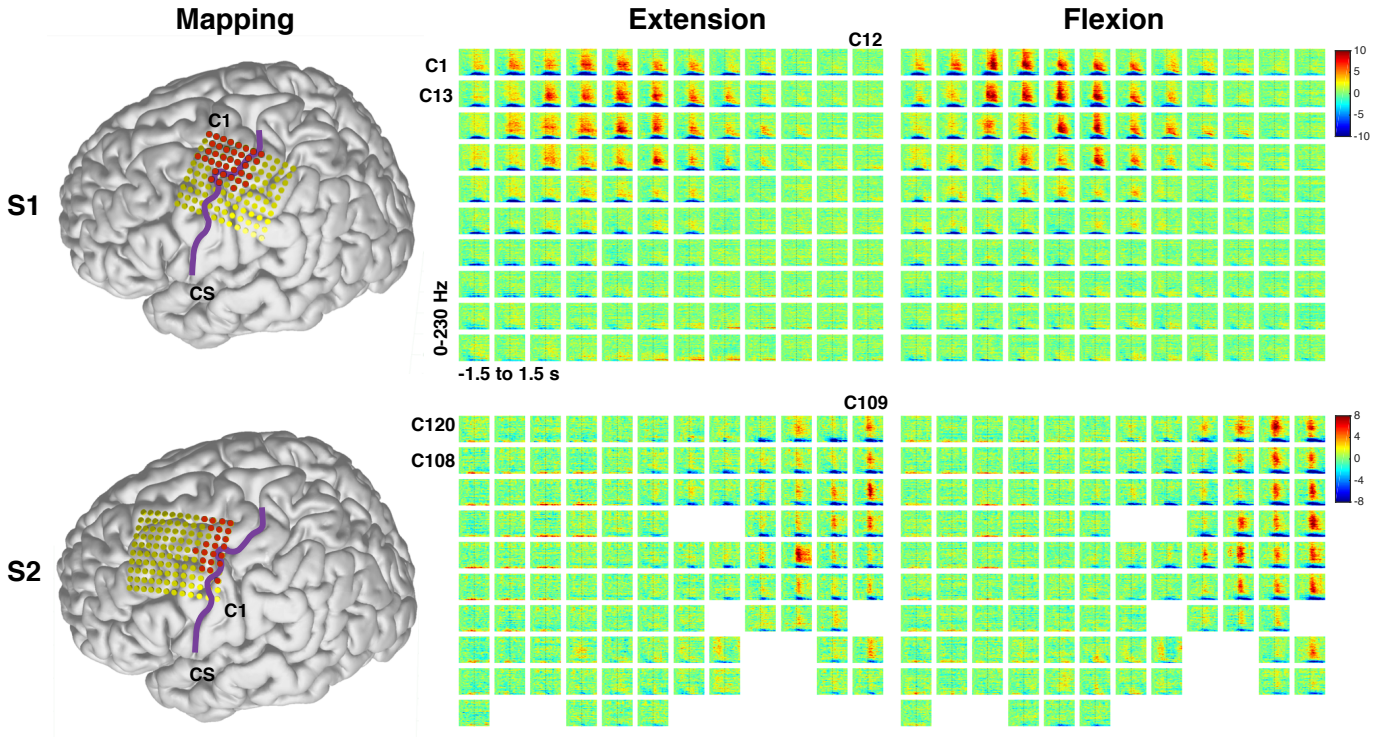

Figure 1. Electrode locations are shown on a 3D rendering of a template brain surface (left). Contacts with clear power increase (ERS) in the high gamma band during movements are marked as red. The central sulcus (CS) is highlighted by a purple line. Each time-frequency map is from -1.5 to 1.5 s, with movement onset at zero second, and covers 0-230 Hz. All maps are displayed in dB scale (S1: -10 to 10, S2: -8 to 8).

1.5s after). After eliminating those segments with artifacts, 25 trials of flexion and 22 trials of extension in total were available for S1. For S2, the total number of trials were 26 and 20 for flexion and extension respectively. Using available trials for each task, an averaged time-frequency map of each channel was computed using short-time Fourier transform (STFT) with 256-sample long Hanning window. The window was shifted with 90% overlap at each step. After computing the averaged time-frequency maps for each channel in hand movement, they were normalized by the average spectrum of the first 500 ms (S_B):

$$S_N = 10 \times \log_{10} \frac{S_A}{S_B} \quad (1)$$

The normalized time-frequency maps were used to inspect the power changes in peri-movement period in different frequency bands. Identified bands were used to quantify the amount of ERD and ERS in each. In this study, ERD was computed in LFB (8-32 Hz) and ERS was computed in HFB (60-200 Hz) based on our observation from time-frequency analysis.

C. Classification

In order to distinguish between the executed tasks, a CSP algorithm was used to extract the spatial patterns of ECoG. CSP is designed to search for an optimal spatial projection that maximizes the variance ratio of projected data between two conditions [10]. Originally implemented in EEG studies to capture the movement related subband power change (LFB-ERD), CSP has been successfully extended to ECoG studies as ERD and ERS were consistently observed in ECoG recordings.

Although both alpha (8-13 Hz) and beta (13-32 Hz) in LFB were associated with ERD, they were usually separately studied as different information conveyed within each subband. In this study, three subbands, alpha (8-13 Hz), beta (13-32 Hz) and gamma (60-200 Hz), were tested for classification. After filtering the data in each subband, averaged spatial covariance matrix was computed for each movement. The optimization problem of CSP can be transformed to the equivalent generalized eigenvalue problem [11]:

$$\Sigma^0 w = \lambda \Sigma^1 w \quad (2)$$

where, w is the generalized eigenvector and λ is the generalized eigenvalue. Σ^0 denotes the averaged covariance of flexion while Σ^1 denotes extension. The variance (energy) ratio between flexion and extension is equivalent to λ here. After obtaining the eigenvalue spectrum, usually a few eigenvectors related to the top and bottom of the spectrum were used for feature extraction [11]. In order to avoid overfitting, we only used two projections, one related to the largest eigenvalue and the other related to the smallest eigenvalue. The two dimensional feature extracted by these two projections was used in LDA for classification. Classification error rates were estimated at each time point using 800 ms of data before that time point. 5×5 cross-validations were performed to generalize the classification accuracies. At each cross validation, the training subset was used to compute the averaged covariance matrices (Σ^0 and Σ^1). In more detail, at each trial, the covariance matrix was computed based on the multi-channel data of 800 ms at specific time point. For each movement, the obtained covariance matrices were averaged across all trials

 ISBN: 978-1-61208-526-5

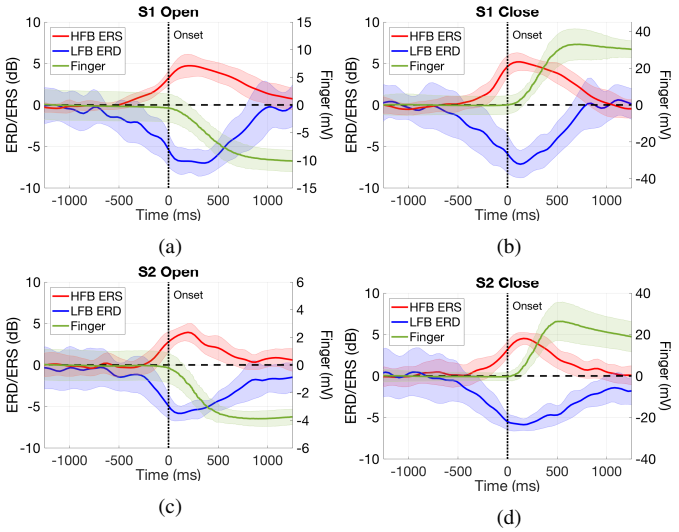

Figure 2. Average ERD (blue) and ERS (red) and average finger positions (green). LFB: 8-32 Hz. HFB: 60-200 Hz. Shaded regions denote the standard deviations across trials.

to yield Σ^0 and Σ^1. After solving Equation 2, the resulting linear projections were used in conjunction with LDA for classification on the test set.

III. Results

The signal analysis and classification results of this study are provided in this section. Specifically, the time frequency analysis of each channel, ERD/ERS analysis and finally the classification results are presented in detail.

A. Time-frequency maps of ECoG grid

The electrode grid was registered onto a template brain surface by comparing the landmarks (central sulcus, midline) of the individual MRI and intraoperative photographs (Figure 1). The normalized time-frequency maps of all channels are displayed on the right side of Figure 1. Although there existed differences between individuals in terms of the level of spectral modulations, for both subjects, we observed clear power decrease in LFB (8-32 Hz) and increase in HFB (60-200 Hz) from sensorimotor areas. ERS in HFB was observed to be more spatially localized while ERD in LFB was more widespread.

B. Event related power changes

ERD in LFB and ERS in HFB from selected channels were averaged and displayed from 1.5 seconds before movement onset to 1.5 seconds after it (Figure 2). Averaged finger positions were also provided in each hand flexion and extension (Figure 2, green). The shaded regions represent the standard deviations across all trials. ERD were observed to have smaller magnitude than ERS in terms of absolute value. Generally, both ERD and ERS happened slightly before the movement onset.

C. Classification

The classification results obtained from three subbands are provided in Figure 3. For both subjects, gamma band

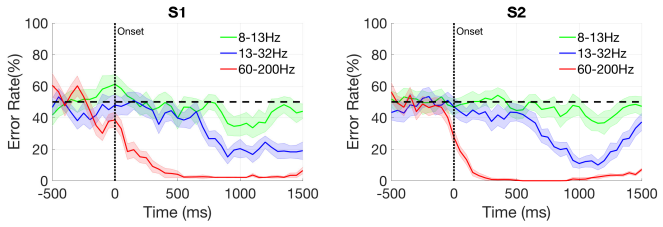

Figure 3. The classification error rates using three different sub-bands: alpha (8-13 Hz, green), beta (13-32 Hz, blue) and high gamma (60-200 Hz, red) in S1 (a) and S2 (b).

consistently yielded better classification results compared to alpha and beta bands. Specifically, in S1, the classification error rate of gamma band at movement onset was 38.54% while alpha and beta band only provided chance level (50%) decoding accuracy. The minimum error rate (2.31%) in S1 was obtained by gamma band at around 500 ms. Both alpha and beta band achieved their maximum classification accuracies at around 1000 ms. However, beta band yielded better classification accuracy compared to alpha band. For S2, the classification error rate at movement onset of gamma band was 27.56% which is clearly better than alpha and beta. Gamma band achieved zero classification error rate at 500 ms. At 250 ms, gamma band already yielded an error rate of 1.82%. Alpha and beta bands reached their best decoding at around 1200 ms. Similar to S1, beta band outperformed alpha band in terms of minimum classification error rate (9.96% versus 36.44%).

IV. Discussion

Neural prosthetics based on ECoG in future can potentially improve the quality of life of paralyzed patients by helping them regain crucial daily hand functions. To our knowledge, for the first time, this study demonstrated the use of ECoG data recorded from a high-density grid to distinguish hand flexion and extension movements of human subjects for a neuroprosthetics. In particular, a high-density ECoG electrode grid (12×10) with 1.2 mm contact size and 4mm spacing was used in this study to investigate cortical activity of hand flexion and extension at very fine temporal and spatial resolution. We decoded the ECoG signal by using the CSP algorithm and LDA to distinguish between executed movements. The decoding system achieved 98-100% discrimination accuracy between hand flexion and extension using the gamma band (60-200 Hz). The classification accuracies in the alpha (8-13 Hz) and beta (13-32 Hz) band were poor and lagged the movement onset dramatically. These results indicated that the gamma band signal from high-density ECoG can be effectively used to differentiate between hand flexion and extension.

Through visual inspection of the time-frequency maps of all channels (Figure 1), ERD in LFB presents similar widespread spatial extent between two tasks while ERS in gamma band is spatially localized and distinct between hand flexion and extension. The most activated ERS channels differ slightly between movements. In addition to the differences in spatial extent, ERS during flexion is also stronger in terms of magnitude compared to extension. The spatial differences together with magnitude differences between movements in gamma band might be utilized by the CSP algorithm to form

 ISBN: 978-1-61208-526-5

an optimal spatial projection that can effectively distinguish between hand flexion and extension.

The best classification accuracies were achieved between 250- 500 ms following the movement onset in both subjects. Since the CSP features are computed in a 800ms window, this might suggest that data from both motor planning phase and execution period contribute to the decoding accuracy. However, as CSP in this study utilized all channels, sensory feedback from those channels located on the sensory cortex might also contribute to the classification results after movement onset. In future studies, CSP needs to be restricted to motor cortex to exclude sensory feedback. We also noticed that ERS in gamma band generally lasts for a few hundred milliseconds (Figure 2) following the movement onset and was stronger during the initiation of the movement but not during the maintenance.

Although the study was executed in two subjects only, we observed that the gamma band consistently yielded almost perfect classification accuracies. Consistently in both subjects, the low band was associated with poor classification accuracies and larger latency. Given the consistent results obtained from both subjects, in the future, our decoding technique based on high-density ECoG can be extended to real-time online decoding applications to establish a hand neural prosthetic.

ACKNOWLEDGMENT

We appreciate the cooperations of our subjects and valuable support of Haidian Hospital in this study.

REFERENCES

[1] W. Penfield and H. Jasper, Epilepsy and the functional anatomy of the brain. Boston: Little Brown, 1954.

[2] A. Palmini, “The concept of the epileptogenic zone: a modern look at Penfield and Jasper’s views on the role of interictal spikes.” Epileptic disorders : international epilepsy journal with videotape, vol. 8 Suppl 2, aug 2006, pp. S10–5. [Online]. Available: http://www.ncbi.nlm.nih.gov/pubmed/17012068

[3] K. J. Miller, M. DenNijs, P. Shenoy, J. W. Miller, R. P. N. Rao, and J. G. Ojemann, “Real-time functional brain mapping using electrocorticography,” NeuroImage, vol. 37, 2007, pp. 504–507.

[4] N. F. Ince, R. Gupta, S. Arica, A. H. Tewfik, J. Ashe, and G. Pellizzer, “High accuracy decoding of movement target direction in non-human primates based on common spatial patterns of local field potentials.” PloS one, vol. 5, no. 12, jan 2010, p. e14384. [Online]. Available: http://journals.plos.org/plosone/article?id=10.1371/journal.pone.0014384

[5] M. G. Bleichner, Z. V. Freudenburg, J. M. Jansma, E. J. Aarnoutse, M. J. Vansteensel, and N. F. Ramsey, “Give me a sign: decoding four complex hand gestures based on high-density ECoG.” Brain structure & function, oct 2014. [Online]. Available: http://www.ncbi.nlm.nih.gov/pubmed/25273279

[6] Y. Nakanishi, T. Yanagisawa, D. Shin, C. Chen, H. Kambara, N. Yoshimura, R. Fukuma, H. Kishima, M. Hirata, and Y. Koike, “Decoding fingertip trajectory from electrocorticographic signals in humans.” Neuroscience research, vol. 85, aug 2014, pp. 20–7. [Online]. Available: http://www.ncbi.nlm.nih.gov/pubmed/24880133

[7] W. Wang, J. L. Collinger, A. D. Degenhart, E. C. Tyler-Kabara, A. B. Schwartz, D. W. Moran, D. J. Weber, B. Wodlinger, R. K. Vinjamuri, R. C. Ashmore, J. W. Kelly, and M. L. Boninger, “An electrocorticographic brain interface in an individual with tetraplegia.” PloS one, vol. 8, no. 2, jan 2013, p. e55344. [Online]. Available: http://journals.plos.org/plosone/article?id=10.1371/journal.pone.0055344

[8] G. Hotson, D. P. McMullen, M. S. Fifer, M. S. Johannes, K. D. Katyal, M. P. Para, R. Armiger, W. S. Anderson, N. V. Thakor, B. A. Wester, and N. E. Crone, “Individual finger control of a modular prosthetic limb using high-density electrocorticography in a human subject,” Journal of Neural Engineering, vol. 13, no. 2, 2016, p. 026017. [Online]. Available: http://stacks.iop.org/1741-2552/13/i=2/a=026017?key=crossref.2d5ef8bc47143308a3a1ff00aabb53dd

[9] T. Jiang, N. F. Ince, T. Jiang, T. Wang, S. Mei, Y. Li, X. Wang, S. Prabhu, and Z. Sha, “Investigation of the spatial and spectral patterns of hand extension/flexion using high-density ECoG,” in 7th International IEEE/EMBS Conference on Neural Engineering (NER). IEEE, apr 2015, pp. 589–592. [Online]. Available: http://ieeexplore.ieee.org/lpdocs/epic03/wrapper.htm?arnumber=7146691

[10] H. Ramoser, J. Muller-Gerking, and G. Pfurtscheller, “Optimal spatial filtering of single trial EEG during imagined hand movement,” IEEE Transactions on Rehabilitation Engineering, vol. 8, no. 4, 2000, pp. 441–446. [Online]. Available: http://ieeexplore.ieee.org/lpdocs/epic03/wrapper.htm?arnumber=895946

[11] B. Blankertz, R. Tomioka, S. Lemm, M. Kawanabe, and K.-r. Muller, “Optimizing Spatial filters for Robust EEG Single-Trial Analysis,” IEEE Signal Processing Magazine, vol. 25, no. 1, 2008, pp. 41–56. [Online]. Available: http://ieeexplore.ieee.org/lpdocs/epic03/wrapper.htm?arnumber=4408441

 ISBN: 978-1-61208-526-5

Incorporate Deep-Transfer-Learning into Automatic 3D Neuron Tracing

Zhihao Zheng and Pengyu Hong
Computer Science, Brandeis University
Waltham, MA, U.S.A
Email: zhihaozh@brandeis.edu, hongpeng@brandeis.edu

***Abstract* — Automated neuron tracing from microscopic images enables high-throughput quantitative analysis of neuronal morphology to elucidate functions of neural circuits. We have developed a transfer-learning approach that trains a deep convolutional neural network to trace neurons in 3D image stacks. Our neural network model consists of two major components. One is responsible for detecting foreground, the other takes the output of the first components and detect the central lines of neurites. They are trained sequentially, which is more efficient than training a whole deep neural network from scratch. The most spectacular aspect of our approach is that our training data is generated by synthesizing 2D simple lines in noisy backgrounds instead of consisting of manually labeled real neuron images which are labor intensive and time consuming to collect. Our method first processes each slices of 3D image, and then integrate them back to produce 3D tracing results. Preliminary test results show that the trained neuron tracer is capable of accurately tracing various types of neurons in noisy images.**

Keywords-Neuron Tracing; Convolutional Neuron Network; Neuron Tracing; Deep Learning, Transfer Learning.

I. INTRODUCTION

It is widely recognized that there is a strong connection between the morphological and functional properties of neurons. The analysis of neuron morphology can shed light on the functional bases of neural systems that consist of various types of neurons connecting with each other. With the rapid advances of imaging technologies, experimental neuroscientists are now able to quickly generate huge volume of 3D neuron images, which demands in-time analysis of neuron morphology. However, manual tracing of neurons in 3D images is time consuming, labor intensive, and often subjective. Hence, it is important to automate neuron tracing to generate accurate results. Digital reconstruction of neurons from microscopic images consists of several major tasks [1] , such as, soma segmentation, neurite tracing, spine segmentation, and so on. In this work, we focus on tracing neurites.

Many automated 3D neuron tracing algorithms have recently been developed [2]-[17] . They are in general capable of accurately tracing neurites. However, each of them relies on some pre-designed models to estimate certain parameters (e.g., foreground thresholds) from images, bridge gaps, or fit certain shape models (e.g., tubes, curves, etc.) to images. It is challenging to design a universal model for microscopic neuron images captured by different imaging instruments under a wide spectrum of setting. Hence, the designs of those models are often based on a small validation set, and can limit the generalization performance of the corresponding neuron tracing methods.

This work was motivated by the incredible capability of an average human being to trace the central lines of general curvature structures in various noisy backgrounds even though this individual never received any special training to perform such a task. We speculated that it might be possible to use simple synthetic stimuli to train a computational model to detect central lines, which can then be applied to trace complex neurite structures. The obvious advantage of this methodology is that we can avoid using intensive and subjective human labors to annotate training data. In this work, we explored the possibility of training the model by Deep Learning [18] and Transfer Learning [19] . We chose Convolutional Neural Network (CNN) [18] , which was biologically-inspired by the groundbreaking work of Hubel and Wiesel on visual cortex [20] , as the base of our Deep-Transfer-Learning network (DTL-NN) model. Our approach first trains a deep neural network to detect foregrounds and central lines in synthetic 2D images (ground truth is trivially known), and then refines the trained model by adding a hidden layer and using a small manually labeled real dataset to make it capable of accurately trace neurons imaged under the desired conditions. Given the 3D image stack of a neuron, we apply a trained DTL-NN to detect central lines of neurites in each 2D image slice. The detected 2D central lines are then pieced together to form the 3D structure of the neuron. Our methodology can not only be used to train neuron tracers, but also be used to build an expandable feature extractor for other complex computer vision problems.

The rest of the paper is organized as the following. In Section 2, we describe the structure of our neural network for foreground detection, centerline extraction and transfer learning. We also explain how to generate the synthetic training dataset, the training procedures, and the post-processing method. In Section 3, we show the experimental results of applying our approach to real datasets. Finally, the paper is concluded with discussions.

 ISBN: 978-1-61208-526-5

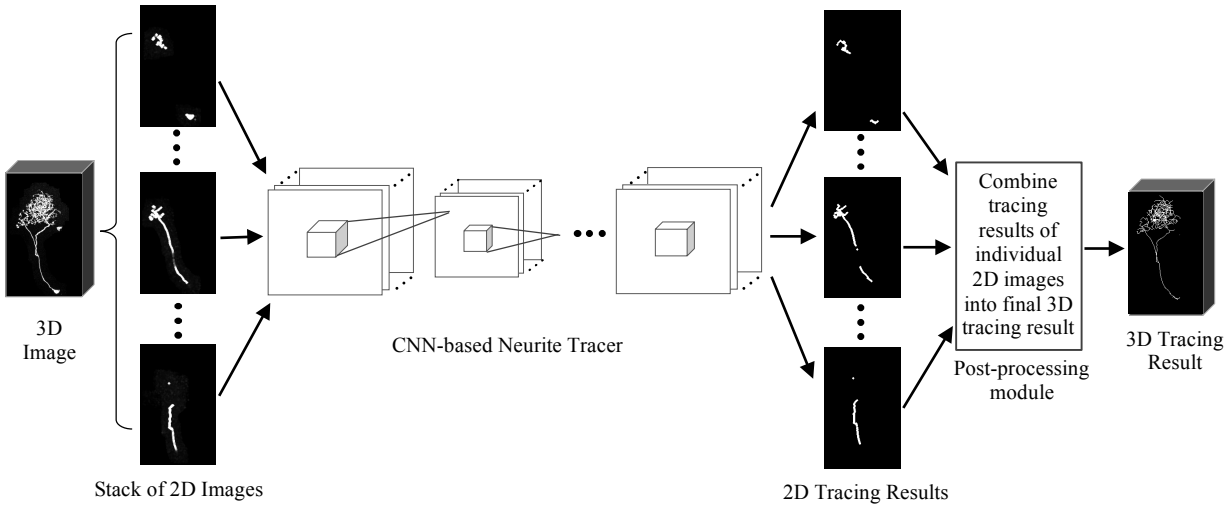

Figure 1. The pipeline of our neuron tracing approach.

II. METHODS

This section describes the technical details of our Deep-Transfer-Learning neural network, the training data, and other key steps of our approach.

A. Overview

Our automated neuron tracing approach (Fig. 1) traces each individual image stack to obtain the intermediate tracing results, which are then combined together by a post-processing procedure to generate the final 3D tracing results. The tracing of individual image stacks is performed by our DTL-NN that consists of three main cascade components, which were trained to detect foreground, extract central lines, and adapt to real images, respectively. Below we explain in details how we effectively train the DTL-NN tracing model using synthetic data and transfer-learning, and how the intermediate tracing results are combined together to produce the final tracing results.

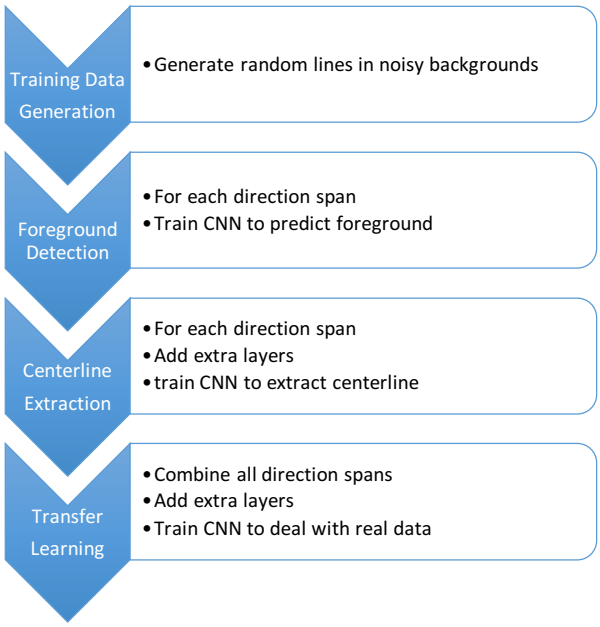

Figure 2. Training procedures of our neural network model.

B. Synthezie Training Data

It is well known that a large training data set of high quality is essential to obtain a superior machine-learning based model. For example, one of the driven forces behind recent striking advances in Computer Vision is high quality manually labelled training sets, such as, ImageNet [21] .

However, the amount of high-quality manually labeled neuron images is highly limited with respect to the almost infinite number of possible experimental conditions and subjects. To deal with this problem, we generated a large-scale training dataset by synthesizing a large number of lines in all directions with different widths and intensities in various noisy backgrounds. The ground truth of this dataset is obviously known. Some examples are shown in Fig. 3. Currently, we only consider lines as the basic structural elements of neurites. In the future, we can include more types of basic structural elements.

C. Train Foreground Detection Module

Foreground detection is a crucial step and can greatly affect downstream analysis. Most neuron tracing methods built their own model for detecting foregrounds manually

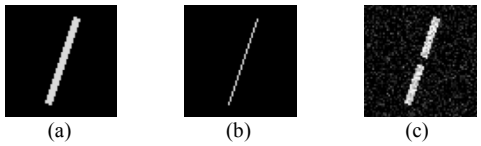

Figure 3. A synthetic training sample. (a) Foreground mask, (b) centerline mask, (c) synthesized image after adding noise to (a).

 ISBN: 978-1-61208-526-5

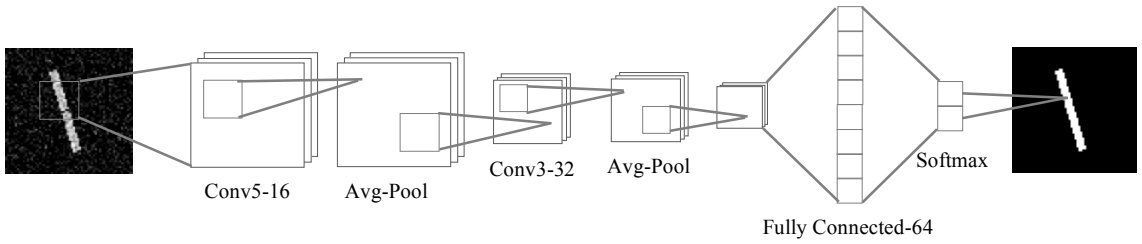

Figure 4. A trial CNN architecture for foreground detection.

(e.g., specify a relatively simple parametric form of the foreground detection models, and the model parameters are either fixed or can be adjusted based on local characteristics of images that can be calculated by some fixed rules). We would like to automatically learn a foreground detection model from data, which can learn to adjust itself to different imaging settings in the future. Initially, we built a large CNN (Fig. 4) for detecting foreground, which however worked relatively poor (Fig. 5b) especially in the areas around bright neurites. We hypothesized that the foreground detection model is able to take better advantage the local structural information, such as, directions. The model in Fig. 3 may be able to learn some local structural information, however, implicitly. In addition, mixing various structural information together makes learning more challenging (i.e., harder to converge to a better solution).

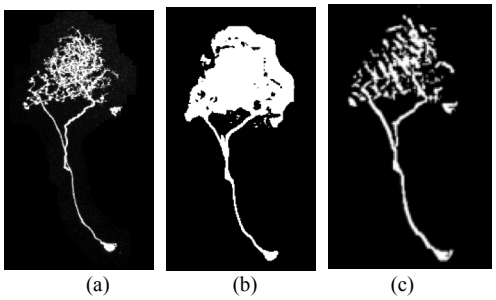

Figure 5. (a) Original image. (b) Foreground detected by the CNN designed in Fig. 4. (c) Foreground detected by the CNN design in Fig. 6.

Therefore, we redesigned our CNN-based foreground detection model (Fig. 6), and explicitly trained it to take advantage of local direction information. We divided all directions into six direction spans: [-22.5° 22.5°], [7.5° 52.5°], [37.5° 82.5°], [67.5° 112.5°], [97.5° 142.5°], and [127.5° 172.5°]. This design mimics the anatomy of the vision neural systems in carnivores and primates, in which neurons with similar direction preferences are clustered into radial columns and are organized in a systematic fashion across the V1 cortical surface [22] .

The synthetic training dataset was also divided into six subsets, one for each direction span. In addition, we design the CNN to consist of six columns, one for each direction span. Each column was pre-trained by using the training subset of the same direction span so that a trained column only responds to the directions within its chosen direction span. All neural network columns were then assembled into one CNN that was fine-tuned using all training data. This

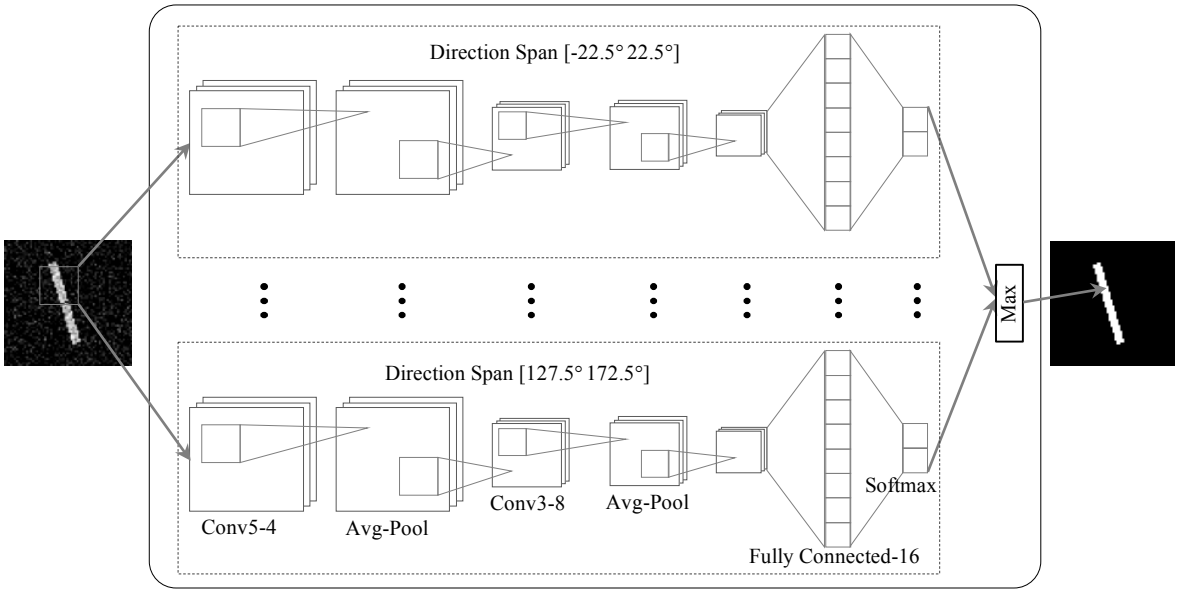

Figure 6. Improved CNN architecture of the foreground detection module.

 ISBN: 978-1-61208-526-5

arrangement sped up the training the whole CNN and produced significantly better results (Fig. 5c). The choice of the spans is based on the window size of our convolution. Since the window size of our first convolution layer is 5 x 5, the minimum angular change it can capture is around 27°. Thus we separated the direction spans by 30° apart. Each direction span covers 45° so that neighboring direction spans have 15° overlap. This non-exclusive design allows the model to better detect lines close to the boundaries of the direction spans.

D. Train Centerline Extraction Module

After obtaining a robust foreground detection module, we trained a centerline extraction module which takes the output of the second-to-the-last layer of the foreground detection module and outputs the corresponding centerline. Basically, we considered the foreground detection module as the feature extractor that learns the intermediate representations of line structures for the centerline extraction module. A fully connected layer was added between the FC-16 and Softmax layers of the foreground detection module (Fig. 7). This modified network was trained to output the centerlines of line structures. We found that it was easier to first train a foreground detection module and then insert a centerline extraction module than to train one big neural network to directly extract centerlines. Comparing the neural network weights of some neurons in the foreground detection module shows that their weights share similar patterns before and after being trained to extract centerlines (Fig. 8). This signals that the neurons in the foreground deteciton module have been appropriately trained during the training step of the foreground detection module.

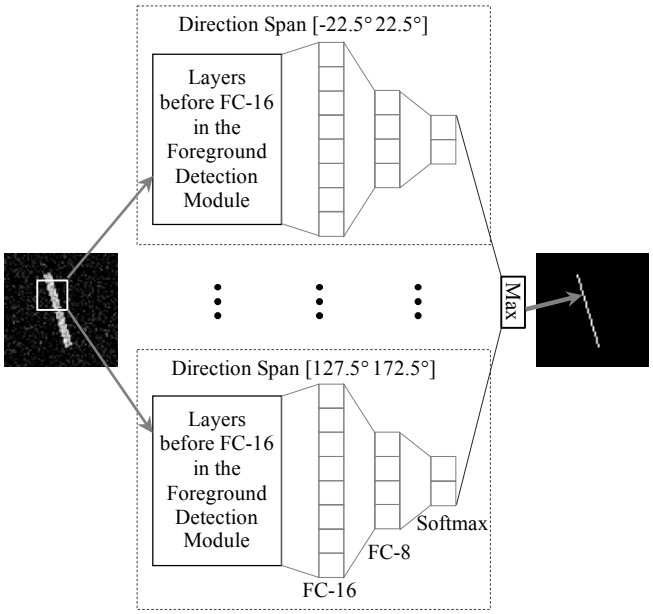

Figure 7. Centerline extraction neural network module.

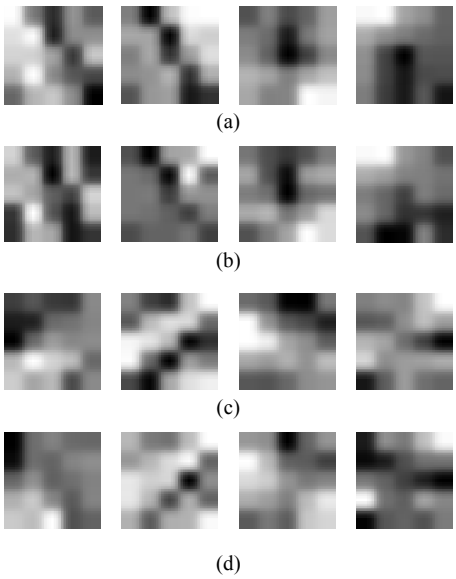

Figure 8. (a) & (c) Weights of a few neurons in the foreground detection CNN responsible for 30° and 150°, respectively. (b) & (d) Weights of the neurons in the centerline extraction CNN corresponding to the neurons in (a) & (c).

E. Adaptation to Real Images and Post-Processing

Previous steps give us a deep neural network that is able to extract central lines of synthetic line structures in noisy backgrounds. More importantly, the deep neural network has learned internal representations for describing various line structures and their centerlines, which can also be very useful, although not perfect, for representing curvature structures in real images. However, real images can have distributions quite different from those in our synthetic training data. To overcome the differences between synthetic images and real images, we apply transfer learning to adapt the trained network to real data by using a small amount of manually labelled real data that are much easier to obtain. In doing this, we use a hidden layer (FC-24) to connect the FC-8 layers of the Centerline Extraction CNN to a Softmax output layer (Fig. 9). This allows us to transfer the knowledge learnt from synthetic dataset to trace neurites in

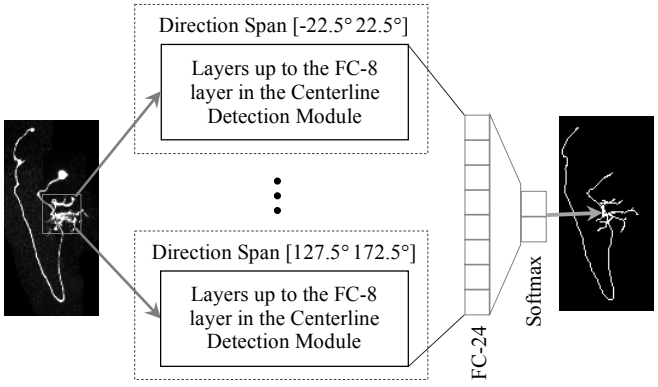

Figure 9. Deep-Transfer-Learning neural network architecture.

real images. The new FC-24 and Softmax layers learns how to utilize the representations learned from synthetic lines and adapt them into new internal representations for processing real data.

Although the model is trained to output 2D centerlines, its outputs are more similar to a shrunk foreground because the model relies on information in local patches and the outputs are softmax results. There is no constraint to force the model to output centerlines with width of exact one. To obtain 3D tracing results, we developed a post-processing module to combine the 2D tracing results of the individual stacks of a 3D image into a 3D tracing result. The post-processing module mainly includes two steps: (a) link the 2D tracing results across stacks based on minimum spanning tree to obtain a 3D map; and (b) apply thinning to the binary 3D map to obtain the final 3D neurite tracing result.

III. EXPERIMENTAL RESULTS

We tested our automated neuron tracing methods on a dataset containing 23 Drosophila neurons provided by the BigNeuron project [23][24] . Typical tracing results (Fig. 10 & 11) show that our model is able to accurately tracing neurons in real 3D microscopic images although it was trained primarily using synthetic data. Our DTL-NN is able to transfer knowledge from synthetic data into real images by adding only one extra hidden layer. The number of parameters added to perform the transfer learning is extremely small (only ~1200 parameters). Hence training of the DTL-NN can be done efficiently.

Table 1 shows the test results computed as the average and standard deviation of pairwise distance from the gold results to our detection results, and pairwise distance from our detection results to the gold results. The errors are mainly caused by the following reasons. First, the resolution sensitivity is reduced by the average pooling layers within the network. Second, some real data contain noise much stronger than what was used in training the network, or some neurites in real data are extremely faint. This led to false positives (i.e., falsely detected neurites) and false negatives (i.e., missed neurites), and hence dramatically increased the detection error. A large-scale experiment is being carried out to thoroughly test this approach.

TABLE I. PAIRWISE DISTANCE WITH GOLD RESULTS

Pair	Pairwise Distance	
	Average	*Standard Deviation*
Gold to Predict	1.363	1.421
Predict to Gold	1.377	1.539

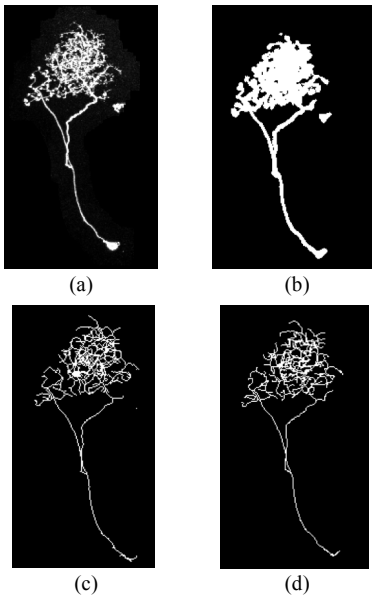

(a) (b) (c) (d)

Figure 10. A tracing example. (a) Original image. (b) Centerline extraction result. (c) Post-processed result. (d) Manually labeled result.

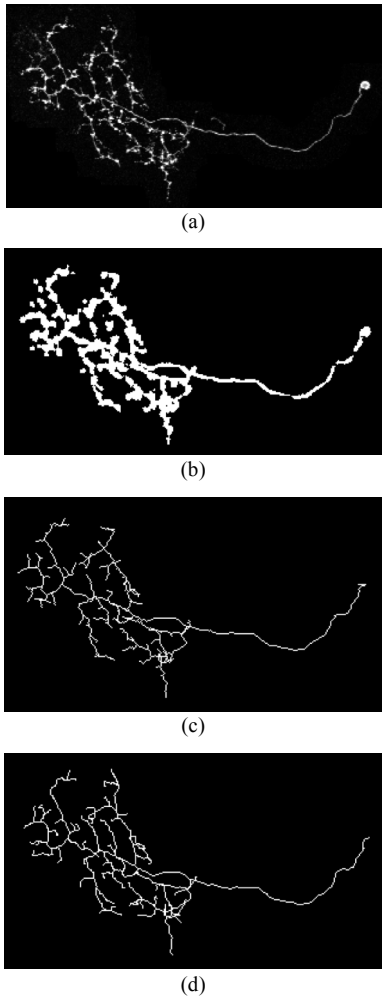

(a) (b) (c) (d)

Figure 11. Another tracing example. (a) Original image. (b) Centerline extraction result. (c) Post-processed result. (d) Manually labeled result.

IV. Conclusion and Future Work

In this paper, we proposed a Deep-Transfer-Learning neural network which is able to learn essential features from synthetic lines and transfers the learnt knowledge to process real neuron images. One major advantage of our approach is that it does not requires a large amount of manually labeled training data. Currently, our approach trains the model to work on 2D images, and use a post-processing step to obtain the final 3D tracing results. We plan to design and train a DTL-NN to directly processes 3D images rather than process each slice, such that we may obtain more accurate 3D features from images than this network. We will also try to design a network, which can involve global information of the image, to further improve our results. More extensive validation tests of our approach will be carried out.

References

[1] E. Meijering, "Neuron tracing in perspective". Cytometry A, 77(7): pp. 693-704. 2010.

[2] K. A. Al-Kofahi, et al., "Rapid automated three-dimensional tracing of neurons from confocal image stacks". IEEE Trans Inf Technol Biomed, 6(2): pp. 171-87. 2002.

[3] S. Schmitt, J. F. Evers, C. Duch, M. Scholz, and K. Obermayer, "New methods for the computer-assisted 3-D reconstruction of neurons from confocal image stacks". Neuroimage, 23(4): pp. 1283-98. 2004.

[4] Y. Al-Kofahi, et al., "Improved detection of branching points in algorithms for automated neuron tracing from 3D confocal images". Cytometry A, 73(1): pp. 36-43. 2008.

[5] B. E. Losavio, et al., "Live neuron morphology automatically reconstructed from multiphoton and confocal imaging data". J Neurophysiol, 100(4): pp. 2422-9. 2008.

[6] H. Peng, Z. Ruan, D. Atasoy, and S. Sternson, "Automatic reconstruction of 3D neuron structures using a graph-augmented deformable model". Bioinformatics, 26(12): pp. i38-46. 2010.

[7] J. Xie, T. Zhao, T. Lee, E. Myers, and H. Peng, "Anisotropic path searching for automatic neuron reconstruction". Med Image Anal, 15(5): pp. 680-9. 2011.

[8] H. Xiao, and H. Peng, "APP2: automatic tracing of 3D neuron morphology based on hierarchical pruning of a gray-weighted image distance-tree". Bioinformatics, 29(11): pp. 1448-54. 2013.

[9] E. Turetken, G. Gonzalez, C. Blum, and P. Fua, "Automated reconstruction of dendritic and axonal trees by global optimization with geometric priors". Neuroinformatics, 9(2-3): pp. 279-302. 2011.

[10] Y. Wang, A. Narayanaswamy, C. L. Tsai, and B. Roysam, "A broadly applicable 3-D neuron tracing method based on open-curve snake". Neuroinformatics, 9(2-3): pp. 193-217. 2011.

[11] A. Choromanska, S. F. Chang, and R. Yuste, "Automatic reconstruction of neural morphologies with multi-scale tracking". Front Neural Circuits, 6: pp. 25. 2012.

[12] X. Ming, et al., "Rapid reconstruction of 3D neuronal morphology from light microscopy images with augmented rayburst sampling". PLoS One, 8(12): pp. e84557. 2013.

[13] S. Basu, B. Condron, A. Aksel, and S. Acton, "Segmentation and tracing of single neurons from 3D confocal microscope images". IEEE J Biomed Health Inform, 17(2): pp. 319-35. 2013.

[14] J. Yang, P. T. Gonzalez-Bellido, and H. Peng, "A distance-field based automatic neuron tracing method". BMC Bioinformatics, 14: pp. 93. 2013.

[15] A. Rodriguez, D. B. Ehlenberger, P. R. Hof, and S. L. Wearne, "Three-dimensional neuron tracing by voxel scooping". J Neurosci Methods, 184(1): pp. 169-75. 2009.

[16] Z. Zhou, X. Liu, B. Long, and H. Peng, "TReMAP: Automatic 3D Neuron Reconstruction Based on Tracing, Reverse Mapping and Assembling of 2D Projections". Neuroinformatics, 14(1): pp. 41-50. 2016.

[17] S. Mukherjee, S. Basu, B. Condron, and S. T. Acton. "Tree2Tree2: Neuron tracing in 3D". in *2013 IEEE 10th International Symposium on Biomedical Imaging*. IEEE. pp. 448-451. 2013.

[18] Y. LeCun, Y. Bengio, and G. Hinton, "Deep learning". Nature, 521(7553): pp. 436-44. 2015.

[19] L. Y. Pratt, S. Hanson, C. Giles, and J. Cowan, "Discriminability-based transfer between neural networks". Advances in neural information processing systems: pp. 204-204. 1993.

[20] D. H. Hubel, and T. N. Wiesel, "Receptive fields and functional architecture of monkey striate cortex". J Physiol, 195(1): pp. 215-43. 1968.

[21] J. Deng, et al. "Imagenet: A large-scale hierarchical image database". in *Computer Vision and Pattern Recognition, 2009. CVPR 2009. IEEE Conference on*. IEEE. pp. 248-255. 2009.

[22] D. H. Hubel, and T. N. Wiesel, "Brain and visual perception : the story of a 25-year collaboration". New York, NY: Oxford University Press, 2005.

[23] A. Jenett, et al., "A GAL4-driver line resource for Drosophila neurobiology". Cell Rep, 2(4): pp. 991-1001. 2012.

[24] H. Peng, et al., "BigNeuron: Large-Scale 3D Neuron Reconstruction from Optical Microscopy Images". Neuron, 87(2): pp. 252-6. 2015.

 ISBN: 978-1-61208-526-5